

Relativistic Effects in Bistatic Synthetic Aperture Radar

Gerhard Krieger, *Fellow, IEEE*, and Francesco De Zan

Abstract—This paper addresses relativistic effects in bistatic and multistatic synthetic aperture radar (SAR) systems and missions. It is shown that the use of different reference frames for bistatic SAR processing and bistatic radar synchronization is prone to notable phase and time errors. These errors are a direct consequence of the relativity of simultaneity and can be explained in good approximation within the framework of Einstein’s special theory of relativity. Using the invariance of the space-time interval, an analytic expression is derived that shows that the time and phase errors increase with increasing along-track distance between the satellites. The predicted errors are in excellent agreement with measurements from TanDEM-X and provide a satisfactory explanation for previously observed digital elevation map (DEM) height offsets that exceeded ± 10 m. Consideration of the unexpected relativistic effects is essential for accurate DEM generation in TanDEM-X and has in the meantime been implemented in the operational processing chain.

Index Terms—Bistatic, interferometry, multistatic, radar-grammetry, relativity, simultaneity, synchronization, synthetic aperture radar (SAR), TanDEM-X.

I. INTRODUCTION

BISTATIC and multistatic synthetic aperture radar (SAR) systems operate with distinct transmit and receive antennas that are mounted on separate platforms. The spatial separation enables new radar imaging modes and is well suited to increase the capability, flexibility, and performance of SAR systems and missions, thereby allowing the acquisition of novel information products [1]–[4]. A prominent example is the TanDEM-X mission, where a global digital elevation model (DEM) is acquired with two X-band SAR satellites flying in close formation [5]. The standard acquisition mode in TanDEM-X is the so-called bistatic mode, where one satellite illuminates the scene with a sequence of radar pulses and both satellites receive the scattered signal echoes from the ground. The simultaneous reception by two receivers makes not only efficient use of the transmitted signal energy but also minimizes the impact of temporal decorrelation.

Manuscript received July 31, 2012; revised January 11, 2013; accepted February 25, 2013. This work was supported in part by the German Federal Ministry for Economics and Technology (Foerderkennzeichen 1072 50 EE 1035).

The authors are with the German Aerospace Center, Microwaves and Radar Institute, 82234 Oberpfaffenhofen, Germany (e-mail: gerhard.krieger@dlr.de; francesco.dezan@dlr.de).

Color versions of one or more of the figures in this paper are available online at <http://ieeexplore.ieee.org>.

Digital Object Identifier 10.1109/TGRS.2013.2251640

The capabilities of bistatic and multistatic SAR missions are accompanied by new challenges regarding radar system implementation, operation, and product generation. Well-known challenges are time and phase synchronization, relative position sensing, selection of appropriate transmitter and receiver trajectories, joint antenna steering, avoidance of mutual irradiation, and bistatic SAR processing [6]–[10]. Up until now, the topics bistatic radar synchronization, relative position sensing, and bistatic SAR processing have been treated almost independently. In doing so, an important aspect has been neglected. Radar time and phase synchronization are typically performed (and thought of) in a platform-based reference frame, while an earth-centered earth-fixed (ECEF) reference frame is usually employed to specify the platform ephemerides and the bistatic SAR processing equations. In this paper, we will show that the unreflected mixture of different reference frames for bistatic SAR data acquisition and bistatic SAR processing may cause notable localization and phase errors in the focused bistatic SAR images. For most bistatic and multistatic SAR systems, these errors can be well approximated and corrected for by considering the space-time relations between two inertial reference frames as established in Einstein’s special theory of relativity. The predicted phase and localization errors and their dependence on the formation geometry are in good agreement with systematic latitude-dependent DEM offsets that have been observed by evaluating a large number of bistatic TanDEM-X data takes.

This paper is organized as follows. Section II explains the difference between the reference frames used for bistatic SAR processing and bistatic radar synchronization. Section III forms the core of this paper and shows the peculiarities that arise if SAR processing and SAR system synchronization are performed in different reference frames. Section IV provides examples from TanDEM-X that illustrate the time and phase errors arising from using different space-time reference frames. This paper concludes with a discussion and a short summary in Sections V and VI, respectively.

II. REFERENCE FRAMES

A. Bistatic Radar Synchronization

A prerequisite for high-quality bistatic and multistatic SAR imaging is an accurate synchronization between the transmitter and receiver radar systems. To this end, several techniques have been suggested, ranging from a tethered radar system over the use of ultrastable clocks up to a direct RF link

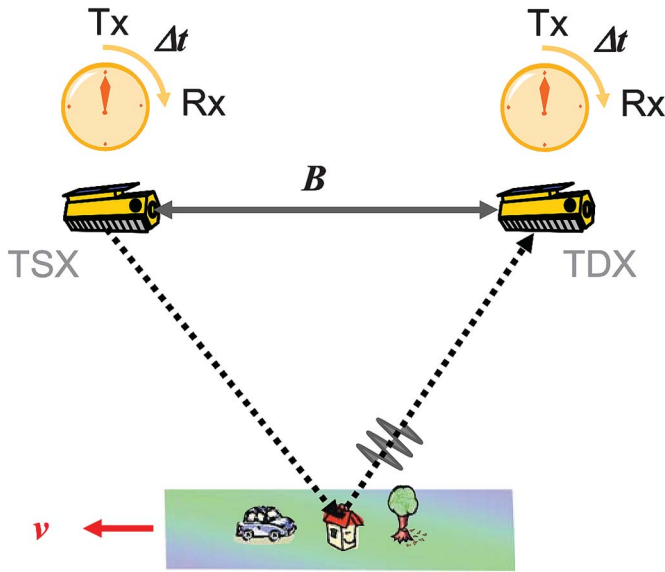


Fig. 1. Bistatic SAR data acquisition as seen from a platform-centered reference frame. The satellites are stationary, while the scene moves with velocity v as indicated by the red arrow. After synchronization, the clocks of the TSX and TDX satellites are assumed to show exactly the same times within this reference frame. A time interval Δt elapses between the transmission of a radar pulse by the TSX satellite and its reception by the TDX satellite.

[11]–[14].¹ A common feature of all these synchronization techniques is that they have the same ultimate goal, namely to establish a common time basis for the transmitter and receiver clocks. A tacit assumption, which was never made explicit, is that the clock synchronization is performed in a reference frame that is linked to the transmitter and receiver platforms. This means that, after synchronization, an observer flying together with the satellites sees all involved clocks showing exactly the same time. We will see later that this may imply that the clocks are no longer synchronous if they are looked at from a different reference frame.

B. Platform-Centered Frame

For the sake of argument, we assume in the following that the transmitter and receiver platforms move with the same constant velocity, so that their positions can be considered stationary in a platform-centered reference frame. We also assume that the transmitter and receiver clocks are perfectly synchronized within the platform-centered reference frame, independent of the actually employed synchronization technique.² Fig. 1 provides an illustration of this situation.

¹In TanDEM-X, a special type of direct synchronization link has been implemented where short radar pulses are periodically exchanged between the two satellites via a pair of preselected horn antennas [5]. An appropriate processing of the synchronization signals allows then the retrieval of the bistatic phase with a relative accuracy in the order of 1° in X-band, a value which has been confirmed during the bistatic commissioning phase of TanDEM-X [15], [16]. This phase accuracy corresponds to a relative time accuracy below 1 ps.

²For this, one may simply think of two highly accurate atomic clocks that are first synchronized at the same position and then slowly separated to the actual platform positions (such a procedure may pose some peculiarities in a noninertial rotating reference frame, the discussion of which is beyond the scope of this paper).

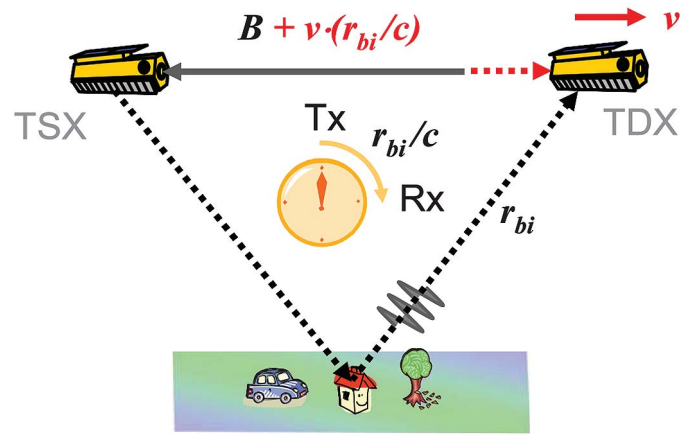


Fig. 2. Bistatic SAR data acquisition as seen from an ECEF reference frame where the scene is stationary and the satellites move.

TSX and TDX denote the transmitter and receiver satellites, which are separated by a constant along-track baseline B . Note that, while the satellites are stationary, the scene on the ground moves relative to this frame with velocity v . In this platform-centered reference frame, the time interval between the transmission and reception of a radar pulse is denoted Δt .

C. Earth-Centered Earth-Fixed Frame

A different picture arises if one considers the bistatic SAR data acquisition from an ECEF reference frame (Fig. 2). The platform ephemerides are typically supplied in this frame, where the earth's surface remains stationary and the satellites are assumed to move along their corresponding trajectories. It is common praxis to provide the full geometric description of the bistatic data acquisition and the associated SAR processing equations in this frame [17]–[21]. Note that the along-track baseline between the satellites differs by $v \cdot (r_{bi}/c)$ from that provided in the platform-centered reference frame if one compares the transmit and receive events. Here, v denotes the receiver velocity, r_{bi} is the bistatic range, and c is the speed of light.

III. RELATIVISTIC EFFECTS

A. Relativity of Simultaneity

In 1905, Albert Einstein propounded his Special Theory of Relativity [22]. According to this theory, the speed of light is an invariant, which means that it always has the same value, independent of the inertial reference frame one uses to describe a physical system. An immediate consequence of this postulate is the so-called nonsimultaneity of events. This means that two spatially separated events which occur at the same time in one reference frame may no longer be simultaneous in another reference frame that moves relative to the first one.

To better understand the relativity of simultaneity and its consequences for bistatic SAR imaging, we consider a gedanken experiment where a virtual “synchronization satellite” is placed in the middle between the TSX and TDX satellites. The objective of the synchronization satellite is to transmit a radar pulse which is then recorded by the two tandem satellites TSX and TDX. Fig. 3 illustrates this situation

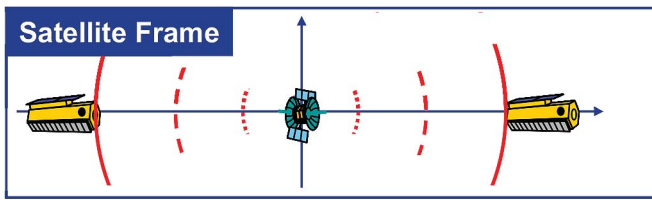


Fig. 3. Illustration of the gedanken experiment. A virtual satellite placed between TDX and TSX transmits pulses (red) that arrive at the same time (i.e., simultaneously) in the platform-centered reference frame.

as seen from a satellite-based reference frame. It is clear that the pulse arrives at TSX and TDX at the same time since the “synchronization satellite” is placed in the middle of the satellite pair.

A concise representation of the previous situation can be obtained by using a space-time diagram as illustrated in Fig. 4. Here, the time axis t is represented by the vertical direction, and two out of the three spatial dimensions are represented by the horizontal x_1, x_2 planes. The left-hand side shows the space-time diagram for the satellite-based reference frame, while the right-hand side shows the space-time diagram for the ECEF frame. The spatial coordinates (x_1, x_2) of the TSX and TDX satellites remain constant within the satellite-based reference frame, whereas they continuously change their positions with time in the ECEF frame.

Let us now assume that, at some time t_0 , a radar pulse (or a set of photons) is transmitted from a virtual satellite located at the midpoint between the two satellites TSX and TDX. In free space (or in any other isotropic medium), the pulse will propagate along a spherical wavefront. This wave propagation is illustrated in Fig. 4 in two spatial dimensions via a red cone.³ According to Einstein’s basic postulate of special relativity, the speed of light (or of any other electromagnetic wave propagation) in empty space is the same for all inertial observers, regardless of the state of motion of the source. This means that the speed of light remains invariant under all linear space-time coordinate transformations. In consequence, the red cone must be the same in both the satellite frame shown on the left of Fig. 4 and the ECEF frame shown on the right. It becomes evident that the pulse arrives simultaneously at the two satellites within the satellite reference frame [Fig. 4(a)]. On the other hand, the pulse arrives first at TDX and only after some delay at TSX if one looks at the same physical situation from the ECEF frame [Fig. 4(b)]. It is hence an inevitable consequence of Einstein’s basic postulate that two events that occur simultaneously within the satellite frame are no longer simultaneous within the ECEF frame. Transferred to bistatic and multistatic SAR imaging, this means that radar transmitters and receivers, which are perfectly synchronous in the platform-centered frame, are no longer synchronous in the ECEF frame where the SAR processing is typically performed. Note that this frame-related effect is completely independent of the choice of synchronization technique, be it a synchronization satellite, the sync-link of TanDEM-X, or any other method. The relativistic effect would even exist if the two satellites transported ultrastable clocks that are synchronized

³In the theory of relativity, this cone is commonly known as the light cone.

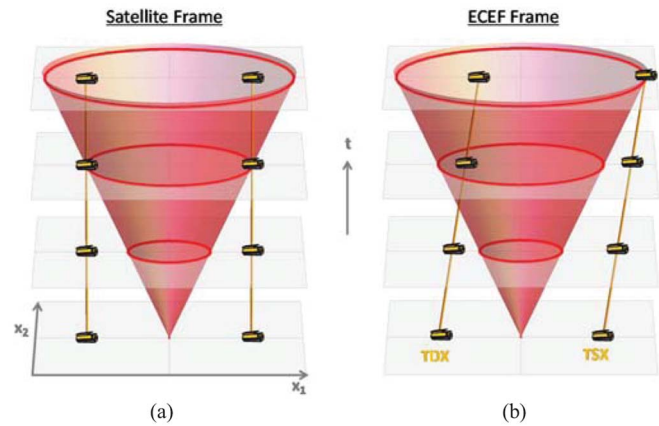


Fig. 4. Space-time diagrams illustrating the nonsimultaneity of events observed from different reference frames. (a) Observation within satellite frame. The spherical wavefront of a pulse emitted from a virtual transmitter (see Fig. 3) arrives at both satellites at the same time. (b) Observation from ECEF frame. The satellites move relative to the ECEF frame, and the wavefront arrives first at TDX and later at TSX.

only once per orbit or ideal identical clocks that needed no synchronization at all.

B. Invariance of Space-Time Interval

In the previous section we have seen that two events that occur at the same time in one reference frame may be no longer synchronous in another reference frame. To quantify the amount of nonsimultaneity, we take advantage of the invariance of the space-time interval which is central to the theory of relativity [23]–[25]. Assuming flat Minkowskian space-time geometry, the space-time interval Δs^2 can be written as

$$\Delta s^2 = (c \cdot \Delta t)^2 - \sum_{i=1}^3 \Delta x_i^2 \quad (1)$$

where Δt and Δx_i denote, respectively, the time and position differences between two events as observed in a given reference frame.⁴ For those with no background in space-time physics, Appendix A has been added to provide a short tutorial derivation of (1). From Fig. 1 it becomes clear that in the platform centred reference frame, the space-time interval between the transmit (Tx) and receive (Rx) events is given by

$$\Delta s^2 = (c \cdot \Delta t)^2 - \|\vec{B}\|^2 \quad (2)$$

where \vec{B} is the baseline vector pointing from the transmitter satellite to the receiver satellite. Using, on the other hand, the ECEF frame of Fig. 2 to describe the same physical situation, the interval between these events is provided by

$$\Delta s^2 = \left(c \cdot \frac{r_{bi}}{c}\right)^2 - \left\|\vec{B} + \vec{v} \cdot \frac{r_{bi}}{c}\right\|^2. \quad (3)$$

By exploiting the invariance of the space-time interval, (2) and (3) can be equated and one obtains

$$(c \cdot \Delta t)^2 - \|\vec{B}\|^2 = \left(c \cdot \frac{r_{bi}}{c}\right)^2 - \left\|\vec{B} + \vec{v} \cdot \frac{r_{bi}}{c}\right\|^2. \quad (4)$$

⁴For those who are familiar with the Lorentz transformations from special relativity, it is straightforward to show that Δs^2 remains invariant under the Lorentz group of linear space-time transformations.

Solving this equation for r_{bi} yields

$$r_{\text{bi}} = \frac{2\bar{B} \frac{\bar{v}}{c} \pm \sqrt{\left(2\bar{B} \frac{\bar{v}}{c}\right)^2 + 4\left(1 - \left(\frac{\|\bar{v}\|}{c}\right)^2\right)(c \cdot \Delta t)^2}}{2\left(1 - \left(\frac{\|\bar{v}\|}{c}\right)^2\right)}. \quad (5)$$

For platform velocities that are small compared to the speed of light, (5) can be well approximated by

$$r_{\text{bi}} \approx c \cdot \Delta t + \bar{B} \cdot \frac{\bar{v}}{c}. \quad (6)$$

The right-hand side of this equation is composed of two terms. The first term represents the product of the speed of light with the time difference between the Tx and Rx events as measured in the platform frame, where radar data acquisition and recording are performed. A user unaware of relativistic effects would mistake this first term as a direct measure of the bistatic range in the ECEF frame. Taking into account the space-time structure of special relativity, the second term emerges. This term is proportional to the scalar product between the platform velocity vector \vec{v} and the baseline vector \vec{B} , i.e., it increases with both the along-track baseline between the satellites and the satellite velocity. For a tandem satellite configuration flying with a velocity of 7.5 km/s and an along-track baseline of 1 km, the second term amounts to a bistatic range error of 2.5 cm. This relativistic range offset may sound small, but for an interferometric X-band system with a wavelength of 3.1 cm, the resulting phase error is with 290° already close to the ambiguity interval.

IV. RELATIVITY IN TANDEM-X

A. DEM Generation With TanDEM-X

TanDEM-X measures for each point on the ground the range difference that arises from its bistatic radar observation from slightly different orbit positions. Via triangulation, it is then possible to derive a digital elevation model of the observed scene. The required range differences can be measured by either evaluating mutual shifts between corresponding pixels of the two acquired radar images or by evaluating their phase difference. The former is known as radargrammetry and its accuracy is essentially limited by the range resolution of the radar. The latter is known as SAR interferometry and it can measure range differences down to a small fraction of the wavelength. By this, a highly accurate DEM with a vertical accuracy on the order of 1 m can be derived. A drawback of the interferometric technique is, however, that the differential range measurement is ambiguous with the wavelength. This ambiguity is resolved by phase unwrapping, which exploits the fact that the topography-induced range difference between neighboring interferometric pixels is typically much smaller than one-half of the wavelength. However, still one vertical reference is required for each acquired scene to determine

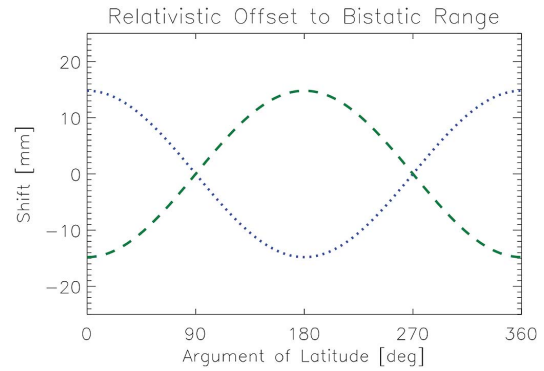


Fig. 5. Predicted relativistic range offset for a typical TanDEM-X satellite formation with a maximum radial displacement of 300 m and a resulting variation of the along-track baseline over ± 600 m. The dashed green curve shows the relativistic offsets if TSX is selected for transmission, while the blue dotted curve shows the predicted offsets in case that TDX is transmitting.

its absolute height.⁵ To avoid such a dependency on external references, TanDEM-X uses in addition radargrammetry to derive the unambiguous height for each scene [26]. The accuracy of the radargrammetric DEM is about two orders of magnitude worse than its interferometric counterpart, but it is nevertheless more than sufficient to resolve the remaining ambiguity in the unwrapped interferogram, since it is possible to average over large areas [27]. Such a strategy to deal without external height references for raw DEM generation is an integral component of TanDEM-X and has proved quite successful (see Section IV-D). An implicit assumption of this approach is, however, that both the radargrammetric and the interferometric techniques provide stable and well-calibrated range and phase measurements without any offset variations between different data takes. As we see in the following, an accurate consideration of relativistic effects will be crucial to achieve this objective.

B. Prediction of Relativistic Range Offsets

In this section, we quantify the predicted relativistic range offsets for TanDEM-X, where the two satellites fly in a close Helix formation [5]. The Helix formation provides not only suitable cross-track baselines for global DEM generation but is also characterized by a periodic variation of the along-track separation B_{along} between the two satellites. For the present context, B_{along} can be approximated with sufficient accuracy by

$$B_{\text{along}}(\Phi) \approx A \cdot \cos(\Phi) \quad (7)$$

where Φ is the argument of latitude and A is a constant that depends on the eccentricity offset between the satellite orbits. Depending on the selected Helix formation, A has typically values between 500 and 900 m.

Fig. 5 shows the predicted relativistic range offsets for TanDEM-X as a function of latitude for $A = 600$ m. Note that

⁵This could, in part, be the DEM from the SRTM mission, which is available for most land surfaces between -56° S and 60° N latitude, while a sufficiently accurate DEM is missing for higher latitudes. Note in this context that some of the calibration strategies established for SRTM are not applicable to TanDEM-X. An example is the use of land sea transitions, which are prohibited in TanDEM-X due to the rather long along-track baselines, causing both decorrelation and differential range offsets in case of water movements.

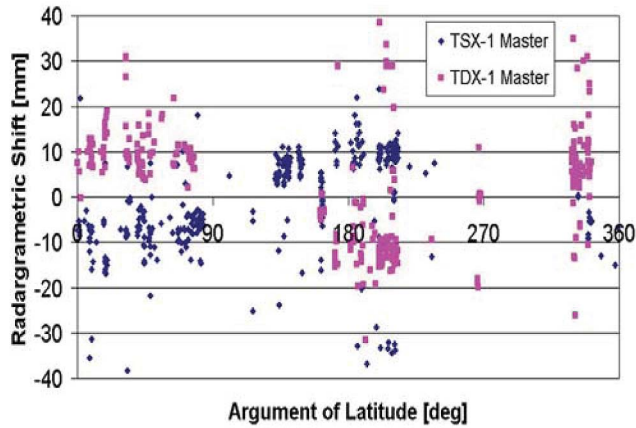


Fig. 6. Measured radargrammetric shifts in TanDEM-X as a function of latitude. The shifts were obtained by comparing TanDEM-X radargrammetric DEMs to reference DEMs [this plot is from the commissioning phase and contains also some other (but smaller) errors that have in the meantime been corrected [30], [31]].

the sign of the shift changes by interchanging the role of the transmitter and receiver satellites. This dependence is evident from both (6) and Fig. 2. The magnitude of the bistatic range error varies between $+15$ and -15 mm. While such an error may be considered small for bistatic localization and image registration, it will cause severe offsets in case of bistatic DEM generation. As noted before, such a DEM can be generated either radargrammetrically or interferometrically by combining the monostatic image from the fully active transmitter with the bistatic image recorded by the passive receiver. Assuming that the relativistic effect can be neglected for the monostatic image, a range difference of ± 15 mm would translate in both cases to a height error of ± 24 m for a TanDEM-X acquisition with a height of ambiguity of 50 m. From this, it becomes clear that relativistic effects cannot be neglected in the operational DEM generation chain of TanDEM-X.

C. Early DEM Processing Results

Fig. 6 shows the estimated radargrammetric offsets for a set of globally distributed data takes. Each measurement point represents the average radargrammetric range offset obtained for a scene with a swath width of approximately 30 km and an along-track extension of 50 km. The offsets were computed by comparing the TanDEM-X radargrammetric DEMs with external reference DEMs. Note that these results had been obtained with an early version of the TanDEM-X processor that did not take into account relativistic effects. The offsets show a characteristic dependence on both the argument of latitude and the master satellite, i.e., the satellite that both transmits and receives. These intricate relations caused great confusion, and any attempts to explain this pattern by remaining internal delays, baseline offsets, etc. failed. For example, an uncompensated difference between the internal delays would mainly cause a constant vertical shift of all measurement points from each master satellite and could neither explain the characteristic latitude dependency nor the striking sign change by switching the master satellite. The same reasoning applies, in principle, to baseline errors. Only after several months of futile search did the idea come up

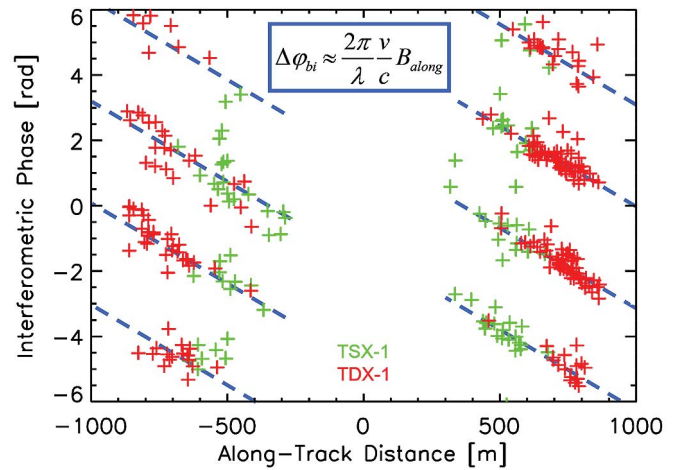


Fig. 7. TanDEM-X interferometric phase offsets as a function of latitude. The relativistic prediction (dashed blue lines) agrees well with the measurements (crosses).

to explain the offsets by relativistic effects. From the theoretical analyses, which had been summarized in the previous sections, it became soon clear that both the magnitude and the characteristic change of sign fit remarkably well with the predicted range offsets from Fig. 5. Note that Fig. 6 is from an early mission phase and still contains some further (but smaller) instrument-related calibration errors that have in the meantime been corrected [30], [31].

Taking into account the relativistic correction and additional calibration steps in the operational TanDEM-X processor, the accuracy of the radargrammetric shifts is now in most cases below ± 5 mm where inaccuracies of the reference DEMs may be the dominant error source.

Fig. 7 shows an even clearer dependence which can be explained by relativistic effects. The red and green crosses denote the interferometric phase offsets that have been obtained by comparing the interferometric TanDEM-X DEMs with reference DEMs.⁶ Besides the π -ambiguity,⁷ which is also resolved in the final processor by radargrammetry, again a clear dependence on the along-track baseline can be seen. By comparing the measured data with the relativistic prediction, which is shown by the dashed blue lines, an excellent agreement is obtained. It becomes again clear that relativistic corrections are required to avoid systematic latitude-dependent offsets in the final DEMs. Note that without the relativistic correction, the interferometric phase values would be almost randomly cluttered among a complete ambiguity interval. As before, this also caused significant confusion within the TanDEM-X engineering team in the beginning.

D. Accuracy Considerations

Several factors influence the accuracy of the absolute height measurements. First, accurate knowledge of the satellite positions is required. Thanks to highly precise double differential GPS evaluations, the relative orbit positions between the

⁶Note that the baseline is always computed from the transmitter (master) satellite, so that the sign flip is not visible in this figure.

⁷The π -ambiguity is a consequence of the bidirectional synchronization technique where the average of two phase values is evaluated.

two TanDEM-X satellites are known with an accuracy of approximately 1 mm [32]. This accuracy has, in the meantime, been confirmed by evaluating periodically repeated DEM acquisitions over a selected set of globally distributed test sites which yielded for the radial and horizontal cross-track baselines standard deviations of 1.1 and 1.3 mm, respectively [33]. Another factor that impacts the absolute height accuracy of the elevation measurements is a difference in the internal delays of the radar hardware of the two satellites. This contribution has also been estimated and corrected for with high accuracy [30]. A further (unexpected) contribution is a differential delay caused by the slightly different signal paths through the troposphere which cause in TanDEM-X incident-angle-dependent height offsets in the order of 1–3 m [34]. Also for this contribution, an appropriate correction has been incorporated in the operational TanDEM-X processor. Further error sources are noise and inaccuracies in the bistatic synchronization system. Here, it was again shown via repeated DEM acquisitions over the same test sites that after accurate calibration, the synchronization accuracy meets (or even exceeds) the specified phase accuracy of 5° [15].

Thanks to the consideration of relativistic effects and the accurate interferometric calibration, it is now possible to meet already for each individual data take the TanDEM-X absolute height error requirement without using any ground references. This greatly facilitates the DEM mosaicking process, and it can be expected that the absolute height accuracy of the final TanDEM-X DEM will be much better than the specified value of 10 m thanks to the bundle block adjustment of multiple data takes [35], [36]. The absolute height accuracy for each individual data take proved also quite helpful to identify potentially inappropriate height references. An example is Greenland, where systematic height offsets in the order of -10 m were observed between the TanDEM-X DEMs and previously acquired ICESat laser altimetry data. Note that such systematic offsets were absent for other areas.

V. DISCUSSION

The relativistic corrections derived in this paper are based on the theory of special relativity, assuming a linear translatory movement between the platform-centered and the ECEF reference frames. To keep the analytic derivation as simple as possible, both reference frames were moreover treated as inertial systems, thereby neglecting secondary effects arising, e.g., from earth's rotation. Strictly speaking, the ECEF reference frame is a rotating coordinate system which is accelerated with regard to an inertial reference frame, thereby causing, e.g., light rays to no longer follow straight lines but curved paths within this reference system. The differential effects from such a deviation are small for close TanDEM-X-like formations, but may become important for future satellite formations employing large cross-track and along-track baselines. In addition, all effects from general relativity, such as gravitational time dilation (or gravitational redshift), which may arise from the formation flying satellites being located on different gravitational potentials, were neglected. While these assumptions are again well justified for the close TanDEM-X formation, such gravitational differences

may become important for bistatic and multistatic constellations that combine SAR satellites in different orbits [6]. An exact and in-depth treatment of these relativistic effects is beyond the scope of this paper and requires advanced mathematics like tensor calculus, differential forms, and the solution of nonlinear differential equations [37]. A detailed investigation of the relativistic effects for large satellite formations and constellations is therefore reserved for a future publication.

VI. CONCLUSION

It has been shown that relativistic effects may cause notable errors in bistatic and multistatic SAR systems and missions. These unexpected errors led to significant confusion when the first bistatic TanDEM-X DEMs were systematically evaluated. Prominent examples were the almost random distribution of the interferometric phase due to its dependency on the along-track baseline and the puzzling sign flip and latitude dependency of the radargrammetric shifts. Both effects could successfully be explained by using the theory of special relativity. The relativistic corrections from this paper have, in the meantime, been incorporated in the operational TanDEM-X processor [29], and the overall spread of the radargrammetric shifts is now well below 10 mm [31].

The relativistic phase and time offsets from this paper are not only of high importance for DEM generation with a formation flying SAR cross-track interferometer. Formations with multiple satellites have also been suggested for a wide range of further remote sensing applications, ranging from along-track interferometry for moving object and ocean current measurements over sparse aperture ambiguity suppression and super resolution for enhanced high-resolution wide-swath SAR imaging up to single-pass SAR tomography for vertical structure measurements [38]–[44]. Due consideration of relativistic effects from varying along-track baselines is again of essential importance for these advanced bistatic and multistatic SAR systems to avoid mutual range and phase offsets between the received SAR signals. The phase accuracy requirements for the combination of the different receiver signals are typically in the order of 1° or a few degrees. For comparison, an along-track baseline of 100 m causes in an X-band system a relativistic phase shift in the order of several tens of degrees. Future multistatic SAR satellite missions should therefore take into account relativistic effects in the design of the radar synchronization system and/or the SAR processor to avoid a possible performance loss.

APPENDIX

This appendix is intended to provide the nonphysicist with a short and easy-to-comprehend introduction to the space-time interval and its invariance under linear space-time coordinate transformations. The basic idea for this derivation is taken from [45]. We consider two events A and B that are separated in space by Δx and Δy and in time by Δt . Let us further assume that the temporal separation Δt between the events is equal to the time it takes for a radar pulse or photon to travel from A to B via a dedicated mirror as illustrated in Fig. 8. The photon's travelled path is shown by the two red arrows,

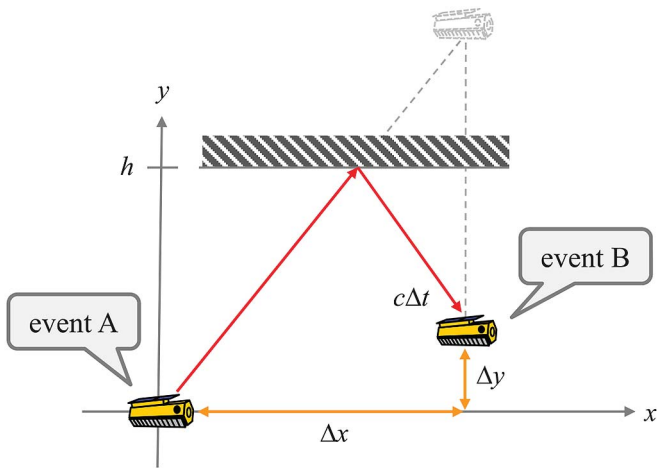


Fig. 8. Derivation of the invariance of the space-time interval. The red arrows show the path of a photon connecting the events A and B via a mirror at vertical position h . The photon's path length $c\Delta t$ can be expressed via the Pythagorean theorem in terms of Δx , Δy , and h as illustrated by the grey dashed lines.

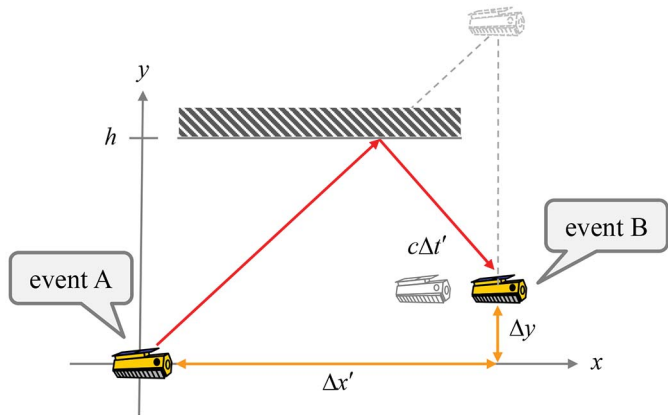


Fig. 9. Derivation of the invariance of the space-time interval. The same physical situation as in Fig. 8 is observed from a different reference frame moving in the x -direction. The photon's path length $c\Delta t'$ can again be expressed via the Pythagorean theorem in terms of $\Delta x'$, Δy , and h as illustrated by the grey dashed lines.

and the overall path length is given by $c\Delta t$. This path length can be computed from the Pythagorean theorem (see grey dashed lines in Fig. 8), taking into account the mirror position h and the spatial separations Δx and Δy between the events A and B as

$$c^2 \Delta t^2 = \Delta x^2 + (2h - \Delta y)^2. \quad (8)$$

We may now look at the same physical situation from another reference frame that moves relative to the previous one in the x -direction. The resulting situation is illustrated in Fig. 9.

Within this second reference frame, the spatial separations between the events A and B are now provided by $\Delta x'$ and Δy . Under the postulate of a constant speed of light, it takes the photon time $\Delta t'$ to travel the path indicated again by the red arrows. As before, we obtain in this second reference frame the relation

$$c^2 \Delta t'^2 = \Delta x'^2 + (2h - \Delta y)^2. \quad (9)$$

Note that we refer in (8) and (9) to the same physical events A and B which are only observed from different reference frames moving relative to each other along the x -axis. We may then resolve (8) and (9) for the term $(2h - \Delta y)^2$ which remains constant for all linear movements along the x -axis and equate both equations to obtain the following fundamental relationship:

$$c^2 \Delta t^2 - \Delta x^2 = c^2 \Delta t'^2 - \Delta x'^2. \quad (10)$$

An extension of (10) to three spatial dimensions and arbitrary linear observer movements yields then

$$c^2 \Delta t^2 - \sum_{i=1}^3 \Delta x_i^2 = c^2 \Delta t'^2 - \sum_{i=1}^3 \Delta x_i'^2 \quad (11)$$

where Δx_i with $i \in \{1, 2, 3\}$ denotes the spatial separation between the two events. The invariant terms on the left- and right-hand sides are commonly known as the space-time interval Δs^2 . The reader interested in a more detailed analytic derivation of (11) may, e.g., consult [46, Ch. I] which proves that the space-time interval remains invariant under linear coordinate transformations.

ACKNOWLEDGMENT

The authors would like to thank the TanDEM-X ITP processing team for providing the radargrammetric and phase offsets and Markus Bachmann for providing Fig. 6. They also wish to thank the anonymous reviewers for their helpful comments.

REFERENCES

- [1] P. Hartl and H. M. Braun, "Bistatic radar in space," in *Space Based Radar Handbook*. Norwood, MA, USA: Artech House, 1989.
- [2] A. Moccia, N. Chiacchio, and A. Capone, "Spaceborne bistatic synthetic aperture radar for remote sensing applications," *Int. J. Remote Sens.*, vol. 21, no. 18, pp. 3395–3414, 2000.
- [3] D. Massonnet, "Capabilities and limitations of the interferometric cartwheel," *IEEE Trans. Geosci. Remote Sens.*, vol. 39, no. 3, pp. 506–520, Mar. 2001.
- [4] G. Krieger, I. Hajnsek, K. Papathanassiou, M. Younis, and A. Moreira, "Interferometric synthetic aperture radar (SAR) missions employing formation flying," *Proc. IEEE*, vol. 98, no. 5, pp. 816–843, May 2010.
- [5] G. Krieger, A. Moreira, H. Fiedler, I. Hajnsek, M. Werner, M. Younis, and M. Zink, "TanDEM-X: A satellite formation for high-resolution SAR interferometry," *IEEE Trans. Geosci. Remote Sens.*, vol. 45, no. 11, pp. 3317–3341, Nov. 2007.
- [6] G. Krieger and A. Moreira, "Spaceborne bi- and multistatic SAR: Potential and challenges," *IEE Proc. Radar, Sonar Navigat.*, vol. 153, no. 3, pp. 184–198, Mar. 2006.
- [7] G. Krieger and M. Younis, "Impact of oscillator noise in bistatic and multistatic SAR," *IEEE Geosci. Remote Sens. Lett.*, vol. 3, no. 3, pp. 424–428, Jul. 2006.
- [8] P. Dubois-Fernandez, H. Cantalloube, B. Vaizan, G. Krieger, R. Horn, M. Wendler, and V. Giroux, "ONERA-DLR bistatic SAR campaign: Planning, data acquisition, and first analysis of bistatic scattering behaviour of natural and urban targets," *IEE Proc. Radar, Sonar Navigat.*, vol. 153, no. 3, pp. 214–223, Jun. 2006.
- [9] I. Walterscheid, J. Ender, A. Brenner, and O. Loffeld, "Bistatic SAR processing and experiments," *IEEE Trans. Geosci. Remote Sens.*, vol. 44, no. 10, pp. 2710–2717, Oct. 2006.
- [10] M. Rodriguez Cassola, S. Baumgartner, G. Krieger, and A. Moreira, "Bistatic TerraSAR-X/F-SAR spaceborne-airborne SAR experiment: Description, data processing, and results," *IEEE Trans. Geosci. Remote Sens.*, vol. 48, no. 2, pp. 781–794, Feb. 2010.
- [11] A. Moccia and S. Vetrilla, "A tethered interferometric synthetic aperture radar (SAR) for a topographic mission," *IEEE Trans. Geosci. Remote Sens.*, vol. 30, no. 1, pp. 103–109, Jan. 1992.

- [12] M. Eineder, "Oscillator clock drift compensation in bistatic interferometric SAR," in *Proc. IEEE Geosci. Remote Sens. Symp.*, Jul. 2003, pp. 1449–1451.
- [13] M. Weiss, "Synchronization of bistatic radar systems," in *Proc. IEEE Geosci. Remote Sens. Symp.*, vol. 3, Sep. 2004, pp. 1750–1753.
- [14] M. Younis, R. Metzger, and G. Krieger, "Performance prediction of a phase synchronization link for bistatic SAR," *IEEE Geosci. Remote Sens. Lett.*, vol. 3, no. 3, pp. 429–433, Jul. 2006.
- [15] *TanDEM-X Science Meeting—Interferometric Performance*. (2009, Oct. 2) [Online]. Available: http://www.dlr.de/Portaldata/32/Resourcen/dokumente/tmx/sciencemeeting3/08-Interferometric_Performance_Handout_small.pdf
- [16] H. Breit, M. Younis, U. Balss, A. Niedermayer, C. Grigorov, J. Hueso Gonzalez, G. Krieger, M. Eineder, and T. Fritz, "Bistatic synchronization and processing of TanDEM-X Data," in *Proc. IEEE Int. Geosci. Remote Sens. Symp.*, Jul. 2011, pp. 2424–2427.
- [17] D. D'Aria, A. Monti Guarnieri, and F. Rocca, "Focusing bistatic synthetic aperture radar using dip move out," *IEEE Trans. Geosci. Remote Sens.*, vol. 42, no. 7, pp. 1362–1376, Jul. 2004.
- [18] O. Loffeld, H. Nies, V. Peters, and S. Knedlik, "Models and useful relations for bistatic SAR processing," *IEEE Trans. Geosci. Remote Sens.*, vol. 42, no. 10, pp. 2031–2038, Oct. 2004.
- [19] R. Bamler, F. Meyer, and W. Liebhart, "Processing of bistatic SAR data from quasi-stationary configurations," *IEEE Trans. Geosci. Remote Sens.*, vol. 45, no. 11, pp. 3350–3358, Nov. 2007.
- [20] Y. L. Neo, F. Wong, and I. Cumming, "A two-dimensional spectrum for bistatic SAR processing using series reversion," *IEEE Geosci. Remote Sens. Lett.*, vol. 4, no. 1, pp. 93–96, Jan. 2007.
- [21] M. Rodriguez Cassola, P. Prats, G. Krieger, and A. Moreira, "Efficient time-domain image formation with precise topography accommodation for general bistatic SAR configurations," *IEEE Trans. Aerosp. Electron. Syst.*, vol. 47, no. 4, pp. 2949–2966, Oct. 2011.
- [22] A. Einstein, "Zur Elektrodynamik bewegter Körper," *Ann. Der Phys.*, vol. 322, no. 10, pp. 891–921, Oct. 1905.
- [23] E. F. Taylor and J. A. Wheeler, *Space-time Physics*. San Francisco, CA, USA: Freeman, 1963.
- [24] R. D'Inverno, *Introducing Einstein's Relativity*. London, U.K.: Oxford Univ. Press, 1992.
- [25] S. M. Carroll, *Space-time and Geometry*. Reading, MA, USA: Addison-Wesley, 2004.
- [26] T. Fritz, C. Rossi, N. Yague-Martinez, F. Rodriguez-Gonzalez, M. Lachaise, and H. Breit, "Interferometric processing of TanDEM-X data," in *Proc. Int. Geosci. Remote Sens. Symp.*, Jul. 2011, pp. 2428–2431.
- [27] C. Rossi, F. Rodriguez Gonzalez, T. Fritz, N. Yague-Martinez, and M. Eineder, "TanDEM-X calibrated raw DEM generation," *ISPRS J. Photogram. Remote Sens.*, vol. 73, pp. 12–20, Sep. 2012.
- [28] A. Renga and A. Moccia, "Performance of stereoradargrammetric methods applied to spaceborne monostatic-bistatic synthetic aperture radar," *IEEE Trans. Geosci. Remote Sens.*, vol. 47, no. 2, pp. 544–560, Feb. 2009.
- [29] T. Fritz, H. Breit, C. Rossi, U. Balss, M. Lachaise, and S. Duque, "Interferometric processing and products of the TanDEM-X mission," in *Proc. IEEE Int. Geosci. Remote Sens. Symp.*, Jul. 2012, pp. 1904–1907.
- [30] J. Hueso Gonzalez, J. Walter Anthony, M. Bachmann, G. Krieger, M. Zink, D. Schrank, and M. Schwerdt, "Bistatic system and baseline calibration in TanDEM-X to ensure the global digital elevation model quality," *ISPRS J. Photogram. Remote Sens.*, vol. 73, pp. 3–11, Sep. 2012.
- [31] M. Bachmann, J. Hueso Gonzalez, G. Krieger, M. Schwerdt, J. Walter Anthony, and F. De Zan, "Calibration of the bistatic TanDEM-X interferometer," in *Proc. 9th Eur. Conf. Synth. Aperture Radar*, Apr. 2012, pp. 97–100.
- [32] A. Jäggi, O. Montenbruck, Y. Moon, M. Wermuth, R. König, G. Michalak, H. Bock, and D. Bodenmann, "Inter-agency comparison of TanDEM-X baseline solutions," *Adv. Space Res.*, vol. 50, pp. 260–271, Jul. 2012.
- [33] J. H. Gonzalez, J. W. Antony, M. Bachmann, G. Krieger, M. Schwerdt, and M. Zink, "Tests of the TanDEM-X DEM calibration performance," in *Proc. Int. Geosci. Remote Sens. Soc.*, Jul. 2012, pp. 303–306.
- [34] G. Krieger, F. De Zan, M. Bachmann, J. Hueso Gonzalez, M. Rodriguez Cassola, and M. Zink, "Unexpected height offsets in TanDEM-X: Explanation and correction," in *Proc. Int. Geosci. Remote Sens. Symp.*, Jul. 2012, pp. 295–298.
- [35] J. Hueso Gonzalez, M. Bachmann, G. Krieger, and H. Fiedler, "Development of the TanDEM-X calibration concept: Analysis of systematic errors," *IEEE Trans. Geosci. Remote Sens.*, vol. 48, no. 2, pp. 716–726, Feb. 2010.
- [36] A. Gruber, B. Wessel, M. Huber, and A. Roth, "Operational TanDEM-X DEM calibration and first validation results," *ISPRS J. Photogram. Remote Sens.*, vol. 73, pp. 39–49, Sep. 2012.
- [37] C. Misner, K. Thorne, and J. Wheeler, *Gravitation*. San Francisco, CA, USA: Freeman, 1973.
- [38] R. Romeiser, M. Schwaebisch, J. Schulz-Stellenfleth, D. Thomson, R. Siegmund, A. Niedermeier, W. Alpers, and S. Lehner. (2002). *Study on Concepts for Radar Interferometry from Satellites for Ocean (and Land) Applications*, Inst. Oceanography, Univ. Hamburg, Hamburg, Germany [Online]. Available: http://www.ifm.zmaw.de/uploads/media/koriolis_cover.pdf
- [39] E. Gill and H. Runge, "Tight formation flying for an along-track SAR interferometer," *Acta Astron.*, vol. 55, nos. 3–9, pp. 473–485, Nov. 2004.
- [40] N. A. Goodman, S. Chung Lin, D. Rajakrishna, and J. M. Stiles, "Processing of multiple-receiver spaceborne arrays for wide-area SAR," *IEEE Trans. Geosci. Remote Sens.*, vol. 40, no. 4, pp. 841–852, Apr. 2002.
- [41] G. Krieger, N. Gebert, and A. Moreira, "Unambiguous SAR signal reconstruction from nonuniform displaced phase center sampling," *IEEE Geosci. Remote Sens. Lett.*, vol. 1, no. 4, pp. 260–264, Oct. 2004.
- [42] D. Cristallini, D. Pastina, and P. Lombardo, "Exploiting MIMO SAR potentialities with efficient cross-track constellation configurations for improved range resolution," *IEEE Trans. Geosci. Remote Sens.*, vol. 49, no. 1, pp. 38–52, Jan. 2011.
- [43] F. Lombardini, "Differential tomography: A new framework for SAR interferometry," *IEEE Trans. Geosci. Remote Sens.*, vol. 43, no. 1, pp. 37–44, Jan. 2005.
- [44] G. Krieger and A. Moreira, "Spaceborne interferometric and multistatic SAR systems," in *Bistatic Radar—Emerging Technology*. New York, NY, USA: Wiley, 2008, pp. 95–158.
- [45] K. Thorne, *Physics in Euclidean Space and Flat Space-time: Geometric Viewpoint* (Lecture Notes), Pasadena, CA, USA: Caltech, 2008.
- [46] B. F. Schutz, *A First Course in General Relativity*, Cambridge, U.K.: Cambridge Univ. Press, 1985.



Gerhard Krieger (M'04–SM'09–F'13) received the Dipl.Ing. (M.S.) and Dr.Ing. (Ph.D.) degrees (Hons.) in electrical and communication engineering from the Technical University of Munich, Munich, Germany, in 1992 and 1999, respectively.

He was with the Ludwig Maximilians University, Munich, from 1992 to 1999, where he conducted multidisciplinary research on neuronal modeling and nonlinear information processing in biological and technical vision systems. Since 1999, he has been with the Microwaves and Radar Institute (HR), German Aerospace Center (DLR), Oberpfaffenhofen, Germany, where he developed signal and image processing algorithms for a novel forward looking radar system employing digital beamforming on receive. From 2001 to 2007, he led the New Synthetic Aperture Radar (SAR) Missions Group, which pioneered the development of advanced bistatic and multistatic radar systems as exemplified by the TanDEM-X mission, as well as innovative multichannel SAR techniques and algorithms for high-resolution wide-swath SAR imaging. Since 2008, he has been the Head of the new Radar Concepts Department, Microwaves and Radar Institute, DLR. He has authored more than 50 peer-reviewed journal papers, seven invited book chapters, about 300 conference papers, and holds five patents. His current research interests include the development of multichannel radar techniques and algorithms for innovative multiple-input, multiple-output SAR systems, the demonstration of novel interferometric and tomographic earth observation applications, and the conceptual design of advanced bi- and multistatic radar missions.

Dr. Krieger was the recipient of several national and international awards, including the W.R.G. Baker Prize Paper Award from the IEEE Board of Directors and the Transactions Prize Paper Award of the IEEE Geoscience and Remote Sensing Society. In 2012, he and his colleagues were nominated for the German President's Award for Technology and Innovation. Since 2012, he has been Associate Editor of the IEEE TRANSACTIONS ON GEOSCIENCE AND REMOTE SENSING, and he will act as the Technical Chair for the European Conference on Synthetic Aperture Radar in 2014.



Francesco De Zan received the Master's degree in telecommunication engineering and the Ph.D. degree with a thesis on SAR interferometry and decorrelating targets from Politecnico di Milano, Milan, Italy, in 2004 and 2008, respectively.

He has collaborated with T.R.E., Milan, on persistent scatterer interferometry and with ESA about the Interferometric Wide Swath Mode of the Sentinel-1 mission during his studies. In 2007, he visited for six months the Stanford Exploration Project at Stanford University, Stanford, CA, USA. He has been with the

Microwaves and Radar Institute of DLR (German Aerospace Center), Oberpfaffenhofen, Germany, since 2008. His current research interests include mission design and performance analysis of future interferometric SAR missions (e.g. BIOMASS, Tandem-L), interferometric/radargrammetric calibration of TanDEM-X, modeling and performance analysis for SAR interferometry, and speckle tracking.